Supplementary Figure 1: A private homozygous essential splicing site mutation of *REL*

(A) Whole-exome sequencing was performed on P. The filtering criteria used for the analysis are indicated. The blacklist is a list of variants that are common (frequency above 1%) in our in-house database of > 9,000 exomes, but absent from public databases (1kG, Exac)[25]. (B) CADD score (*y*-axis) plotted against minor allele frequency (MAF, *x*-axis) for the variants present in the gnomAD database (http://gnomad.broadinstitute.org). Heterozygous missense variants are shown as black circles, predicted heterozygous loss-of-function variants are shown as open circles, homozygous variants are shown in blue, and the essential splice variant studied here is depicted in red. (C) Consensus negative selection score (CoNeS)[28] of *REL* and its distribution for genes causing inborn errors of immunity (IEI), according to disease mode of inheritance (AD: autosomal dominant, AR: autosomal recessive).

Supplementary Figure 2: The c.395-1G>A mutation alters *REL* mRNA splicing with no leakiness

(A) Total mRNA extracted from EBV-B cells from controls, P's mother (m/wt) and P, was subjected to RT-PCR for the full-length *REL* cDNA. (B) Insertion of wild-type (WT) and mutant (c.395-1G>A) *REL* genomic DNA segments into the pSPL3 plasmid for the in vitro exon trapping experiment. (C) Agarose gel electrophoresis showing PCR-amplified spliced variants from COS7 cells not transfected (NT), or transfected with empty pSPL3 (EV), or pSPL3 containing the *REL* c.395-1G>A, or the wild-type *REL* genomic DNA sequence. (D) The PCR products obtained in (C) were subjected to TA cloning and Sanger sequencing. The percentages of the different spliced variants (V1-V5) generated from the WT *REL* or c.395-1G>A *REL* clones are shown.

Supplementary Figure 3: No c-Rel protein is detected in the patient's cells

c-Rel protein levels in EBV-B cells, as assessed by western-blot analysis on total cell extracts (A) and by intracellular flow cytometry (B), for controls (Ctls; *n*=2), P and her mother (m/wt). A mAb against the residues surrounding the Leu65 residue of c-Rel was used for western blotting. A polyclonal Ab against the C-terminal part of c-Rel was used for flow cytometry. Representative results from three independent experiments are shown. (C) Flow cytometry histograms showing c-Rel expression in leukocyte subsets, as assessed by intracellular flow cytometry on PBMCs from one representative control (Ctl) and P. (D) c-Rel protein levels in leukocyte subsets, as assessed by flow cytometry on fresh PBMCs from controls (*n*=10). Mean fluorescence intensity (MFI) for c-Rel is shown for the various leukocyte subsets, relative to an isotype control. Mean ± SEM.

Supplementary Figure 4: Immunophenotyping

Dot-plot graphs are presented. All analyses were conducted after the exclusion of dead cells from PBMCs isolated from healthy controls (Ctls) and P tested on two different dates, except for innate lymphoid cells (ILC). The horizontal bars represent the median. (A) ILC phenotyping, showing the frequencies of total helper ILCs (Lin^- $CD7^+CD56^-CD127^+$), and of ILC precursors ($CD117^+$), ILC1 ($EOMES^-IFN\text{-}\gamma^+$), and ILC2 ($GATA3^+IL\text{-}13^+$), among the $CD45^+$ cells. (B) Phenotyping of NK cells, showing the frequency of $CD56^{bright}$ cells among total NK cells ($CD3^-CD56^+$), and terminal differentiation profile in the $CD56^{dim}$ compartment, as assessed by the distribution of NKG2A and KIR, in controls (*n*=38) and P.

Supplementary Figure 5: Transcriptomic profile at single-cell level in vivo is not altered in c-Rel deficiency

(A) Dot-plot graphs showing the proportions of cells for the major clusters identified by scRNA-seq. (B) Volcano plot showing the results of a differential gene expression analysis for P vs. control cells for the major cell clusters identified in A.

Supplementary Figure 6: c-Rel deficiency affects the production of IL-12 and IFN-γ

(A) ELISA data for whole-blood activation are shown. IL-12p40 production in whole blood from healthy controls (*n*=10) and P, after incubation for 48 h with different ligands. BCG: *Bacillus* Calmette-Guerin, PMA/Iono: PMA+ionomycin. Mean ± SEM. *N*=3. (B) ELISA data for in vitro-derived CD141c$^+$ cDC1 and CD1c$^+$ cDC2 from purified CD34$^+$ stem cells isolated from healthy controls (*n*=3) and P. IL-12p40, IL-12p70, IL-23, and CXCL10 production after 48 h of incubation with a combination of BCG+IFN-γ. Mean ± SEM. *N*=1 (C) ELISA data for in vitro-derived monocytes from purified CD34$^+$ stem cells isolated from healthy controls (*n*=3) and P. IL-12p40, IL-23, and IL-1β production after 48 h of incubation with LPS. Mean ± SEM. *N*=1. (D) ELISA data for EBV-B-cell activation are shown. Production of IL-12p40 by cells from P, not transfected (NT), or transfected with an empty retroviral plasmid (EV), or a plasmid encoding the wild type c-Rel (WT); by cells derived from patients with complete AR IL-12p40 deficiency (*n*=2); and by cells derived from healthy controls (Ctls; *n*=3). Cells were incubated with PDBu (10^{-7} M) or PMA (400 ng/ml) for 24 h. Mean ± SEM. *N*=3. (E) IFN-γ expression after 24 hours of stimulation in distinct leukocyte subsets defined by surface markers (details provided in the methods section) for 11 controls, 1

patient with AR IL-12Rβ1 deficiency and P. Dot-plots graphs are shown. Bars represent the mean and SD. Technical replicates are shown for P.

Supplementary Figure 7: The surface expression of costimulatory molecules is intact on in vitro-derived c-Rel-deficient myeloid cells

The expression of HLA-DR, CD80, CD83, and CD86 was measured on the surface of $CD303^+$ pDC, $CD1c^+$ cDC2, and $CD141^+$ cDC1, derived in vitro from purified $CD34^+$ stem cells from healthy controls (*n*=3) and P. (A) Flow cytometry histograms are shown for one representative control and P. (B) Mean fluorescence intensity (MFI) relative to an isotype control for each co-stimulatory molecule is shown for the various DC subsets. *N*=2. Mean ± SEM.

Supplementary Figure 8: c-Rel deficiency impairs the upregulation of costimulatory molecules on peripheral cDCs and contributes to poor T-cell responses to antigen

PBMCs from healthy controls (*n*=3) and P were incubated with the indicated ligands for 12 h. Surface expression of CD80 (A) and CD40 (B) was assessed on $CD19^+CD27^-$ naïve B cells. Histograms and the mean fluorescence intensity (MFI) of CD80 and CD40 expression are shown. (C) CFSE-stained PBMCs from P were cultured for seven days under Th0 conditions; or with sorted $Lin^-HLA\text{-}DR^+CD11c^+$ cDCs from a heathy control (cDC HD) or P's mother (cDC het) in two different proportions (0.5% or 10%), ± various doses of IL-2 (ng/ml) or tuberculin (PPD; 5 μg /ml). Flow cytometry plots of CFSE dilution were obtained for viable $CD4^+$ T cells, and data for the absolute number of dividing cells were analyzed. *N*=1

Supplementary Figure 9: c-Rel deficiency impairs T-cell proliferation, IL-2 production and effector function

Fresh PBMCs from healthy controls (results for one control are shown) and P were incubated for four days with beads coated with anti-CD3/CD28 mAbs; in Th0 conditions; or with PHA (1 µg/ml) ± IL-2. Flow cytometry histograms showing proliferation, as measured by CFSE dilution for $CD8^+$ T cells (A) and CD25 expression (B), and bar graphs showing the absolute number of live $CD4^+$ T cells (C). (D) Fresh PBMCs from four healthy controls and P were cultured for six hours with anti-CD3/CD28 mAbs; or PMA (20 ng/ml) and ionomycin (10^{-5}M). Data for the expression of IFN-γ and TNF are shown. (E) IL-2 production by sorted naïve $CD4^+$ T cells from controls (*n*=6) and P was measured after five days of culture under Th0 conditions. Mean ± SEM. ELISA data representative of two independent experiments are shown. (F) Sorted naïve $CD4^+$ T cells from controls (*n*=4) and P were incubated for four days under Th0 conditions + IL-2. Flow cytometry analyses of CFSE dilution were performed and the percentage (%) of cells in each division was analyzed. Mean ± SEM. Representative results from two independent experiments are shown. (G) RT-qPCR was performed on mRNA extracted from sorted naive $CD4^+$ T cells from controls (*n*=5) and P cultured under Th0, or Th1 or Th17 polarizing conditions. *N*=1. (H) Cytokine expression by sorted memory $CD4^+$ T cells from controls (*n*=8) and P was measured after five days of culture under Th0 conditions. N=2. Mean ± SEM.

Supplementary Figure 10: c-Rel regulates the expression of a restricted set of genes at early stages of $CD4^+$ T-cell activation

(A) Dimension-reduction analysis (partial least-squares method) comparing the normalized RNA-seq gene expression values of untreated and stimulated (anti-CD2, -CD3, -CD28, -CD3/CD2, -CD3/CD28 mAb, or PMA) naïve $CD4^+$ T cells recovered from four healthy donors and P. (B) Heatmap representing the log2-fold change (log2FC) of expression between the stimulated naïve $CD4^+$ T-cell samples and their corresponding unstimulated samples. We included four stimulations: anti-CD3, -CD3/CD2, -CD3/CD28 mAb, and PMA. We stimulated four control samples and the patient's sample with each agent. Only the genes that are differentially expressed (adjusted $P < 0.05$ and $| \log2FC | > 1$) between the unstimulated controls and at least one of the groups of stimulated controls are included. (C) Graph showing the normalized ChIP-seq peak height for c-Rel in naïve $CD4^+$ T cells before and after stimulation with PMA. (D) RT-qPCR performed two hours after the activation of purified naïve $CD4^+$ T cells from four healthy donors and P with anti-CD3 mAb with or without anti-CD28 mAb. The data shown are $2^{-\Delta\Delta Ct}$ values. Error bars represent the SD.

Supplementary Figure 11: The B-cell response is impaired by c-Rel deficiency

(A) Naïve B cells from controls (*n*=20) and P were sorted and cultured with CD40 ligand (CD40L), alone or in combination with anti-IgM mAb and CpG or IL-21 for seven days. The secretion of IgG and IgA was then assessed by IgH chain-specific ELISA. *N*=2. Mean ± SEM (B) Naïve B cells from two representative controls and P were sorted, labeled with CFSE, and incubated with the indicated ligands. Proliferation (CFSE dilution) and viability (Zombie staining) were measured after four days. (C-D) Naïve $CD4^+$ T cells from controls (*n*=3) and P were sorted and cultured under Th0 conditions for three days. The surface expression of ICOS and CD40L was measured after

three days. *N*=1. Mean ± SEM. (E) IL-21 expression by sorted naive $CD4^+$ T cells from controls (*n*=11) and P, cultured under Th0 or Th1 polarizing conditions, was measured after five days. Mean ± SEM. *N*=3.

Supplementary Figure 12: c-Rel deficiency compromises the expression of CD40-dependent target genes involved in naïve B-cell maturation

(A) Heatmap representing the log2-fold change (log2FC) of expression between the stimulated naïve B-cell samples and their corresponding unstimulated samples. We included three stimulations: $F(ab')_2$ goat anti-human IgM (anti-IgM), CD40 Ligand (CD40L) and PMA. We stimulated four control samples and the patient's sample with each agent, as well as a patient with CD40 deficiency. Only the genes that are differentially expressed (adjusted $P < 0.05$ and $|log2FC| > 1$) between the unstimulated controls and at least one of the groups of stimulated controls are included. (B) Flow cytometry histograms showing c-Rel (left panel) and CD271 expression (right panel) in EBV-B cells from P either not transduced (NT), or transduced with an empty retrovirus (EV) or with a plasmid encoding the wild-type c-Rel (WT). c-Rel expression was assessed by intracellular flow cytometry on non-transduced, and transduced cells. CD271 expression is shown as a control for transduction with the retroviral plasmid. (C) Graph comparing the normalized c-Rel ChIP-seq peak height in naïve B cells before and after stimulation with CD40L plus anti-IgM.

Supplemental Figure 1.

A.

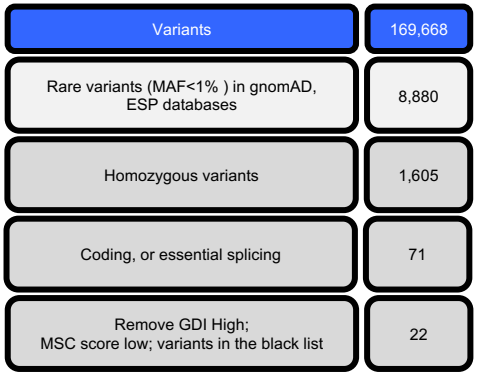

B.

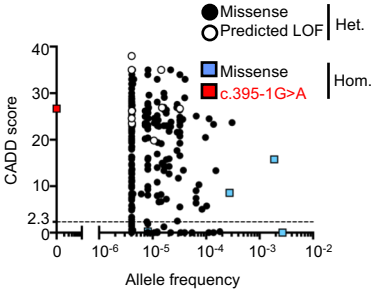

C.

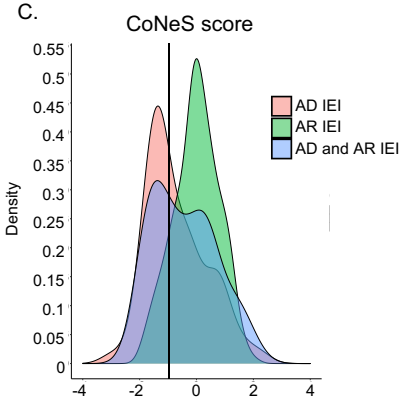

Supplemental Figure 2.

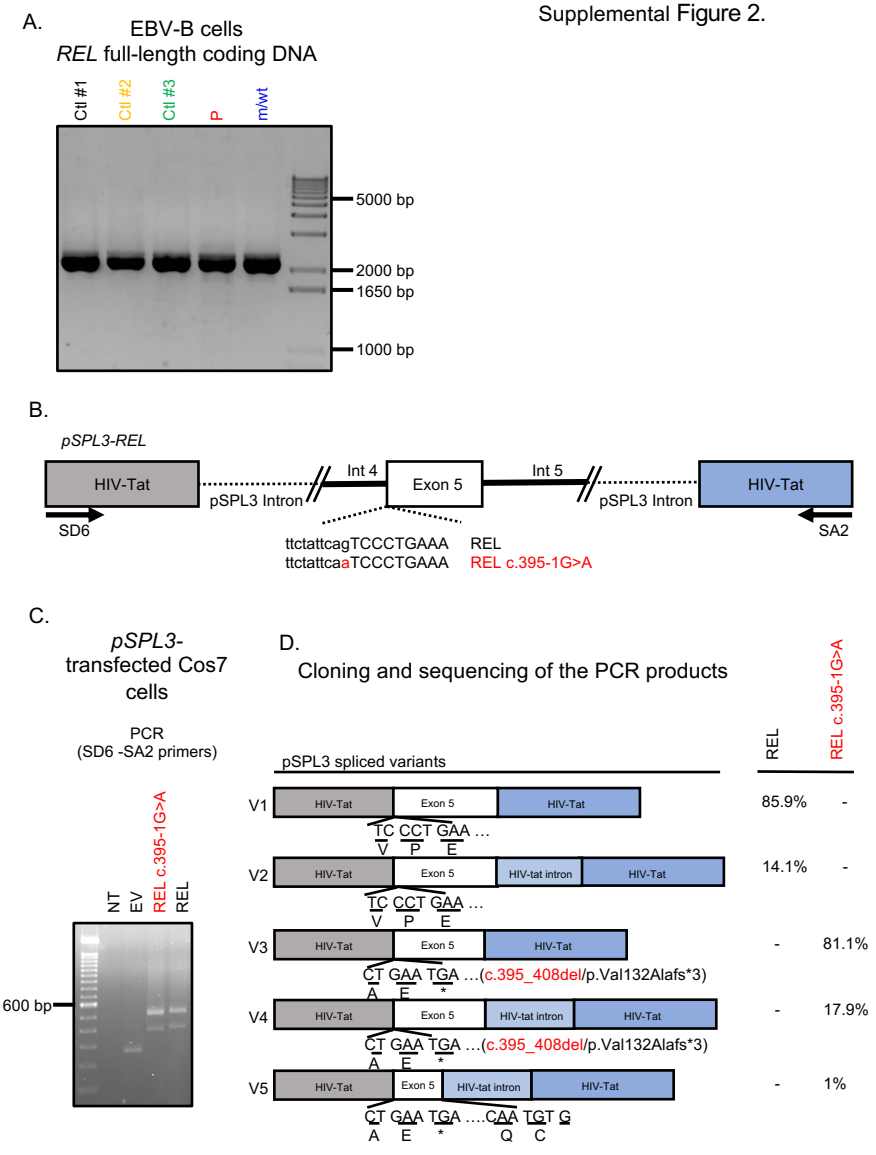

Supplemental Figure 3.

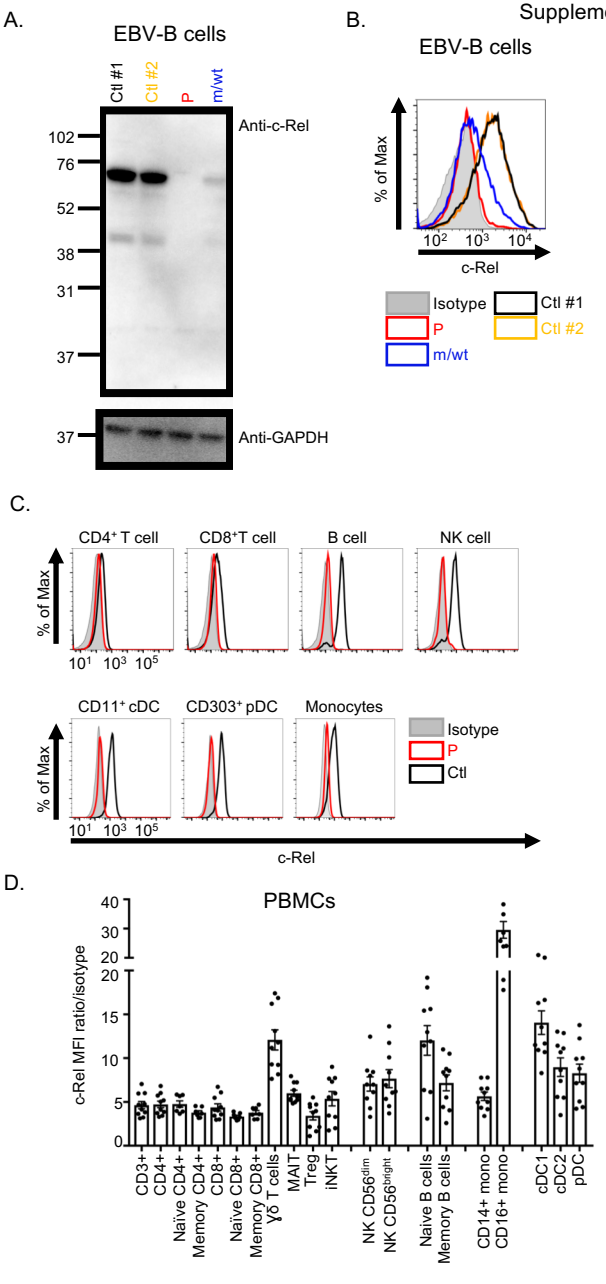

Supplemental Figure 4.

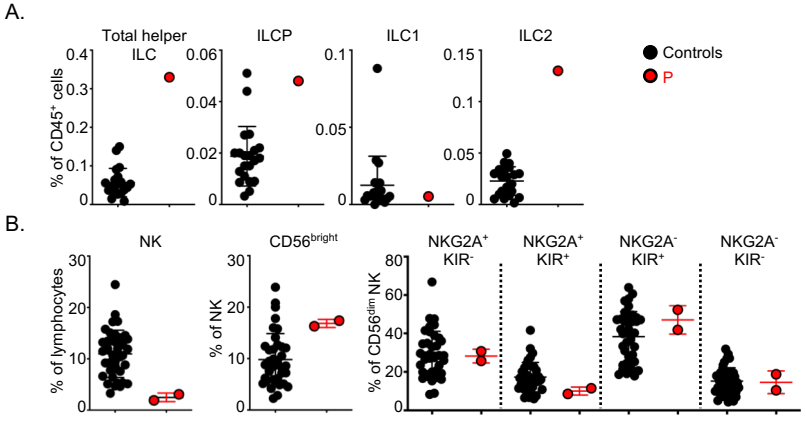

Supplemental Figure 5.

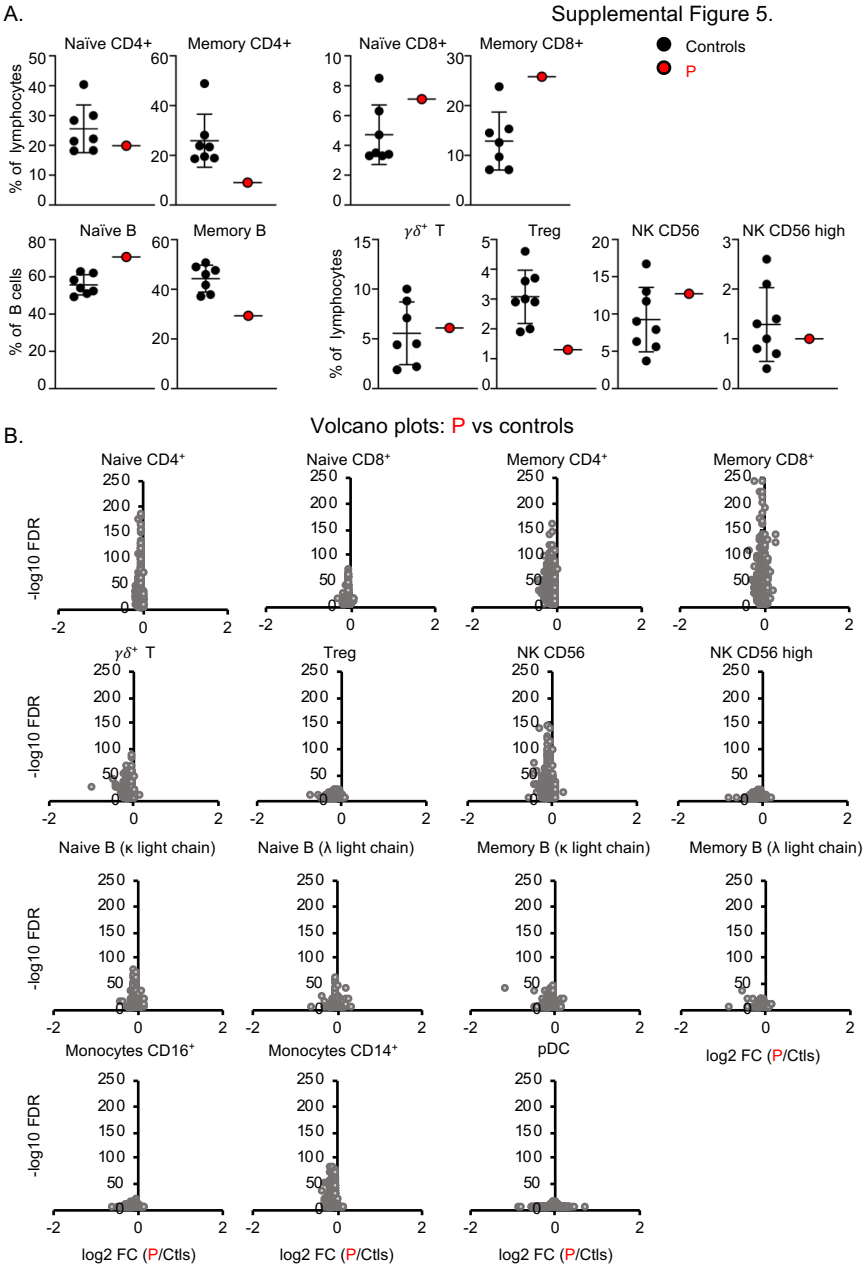

Supplemental Figure 6.

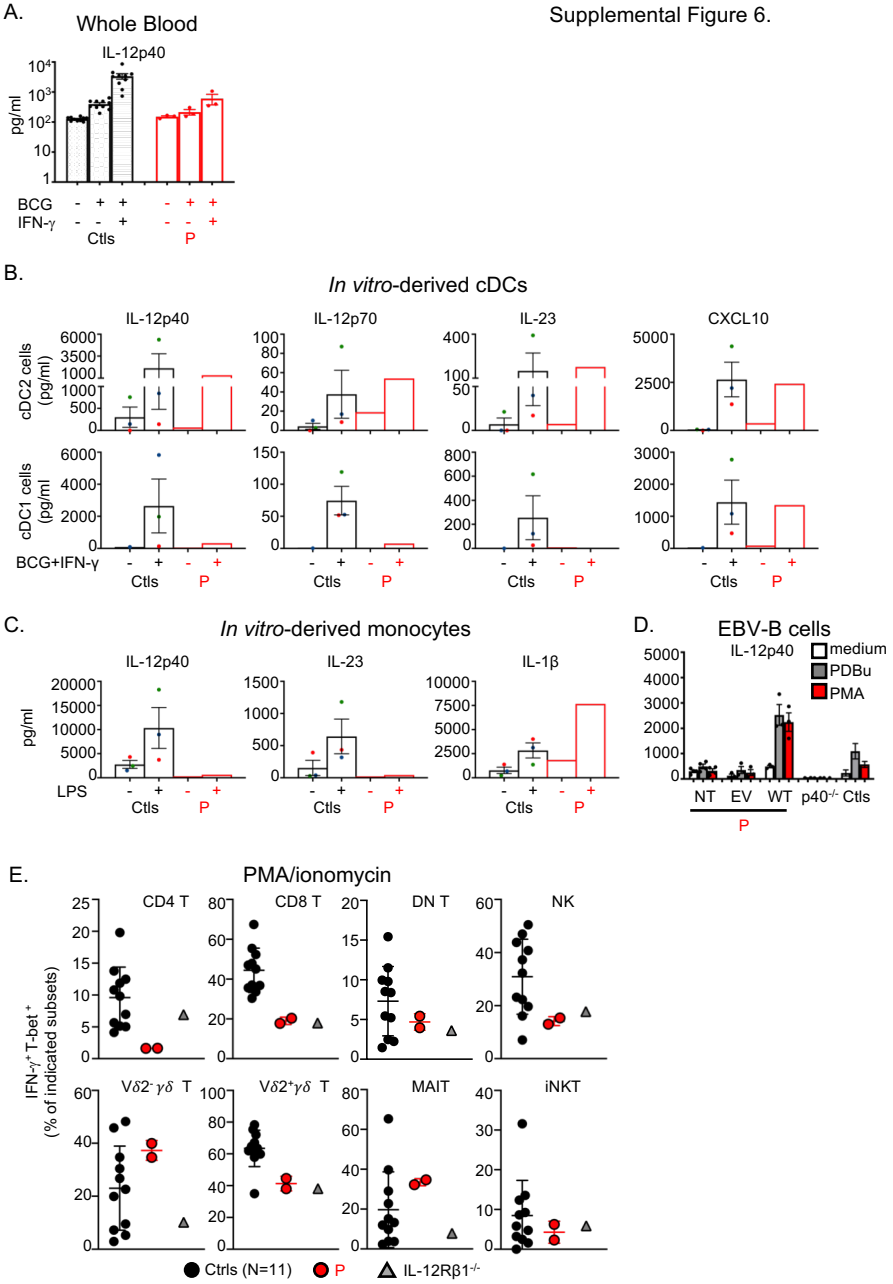

Supplemental Figure 7.

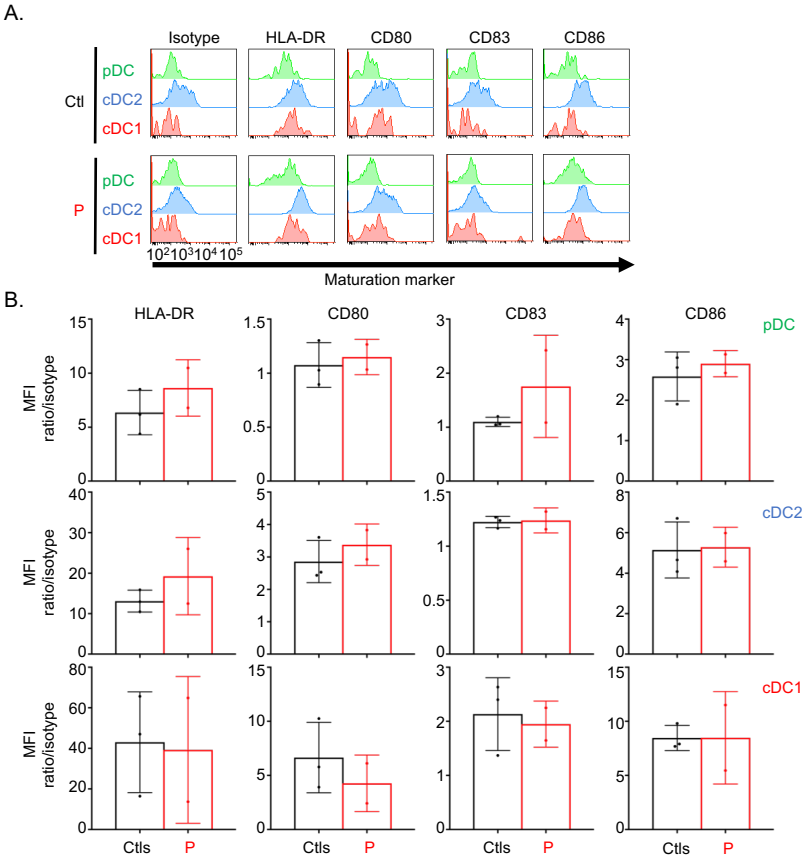

Supplemental Figure 8.

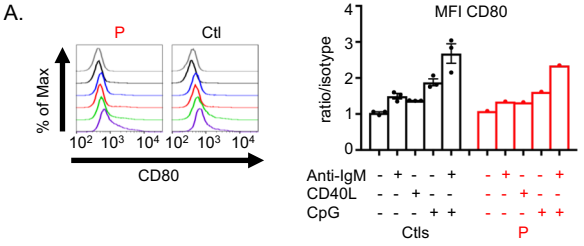

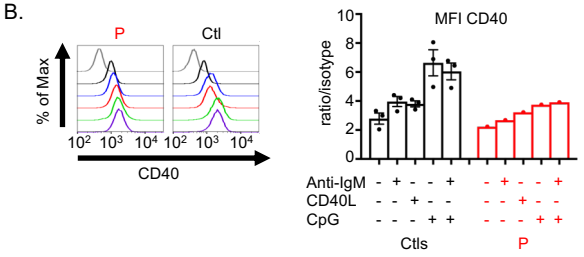

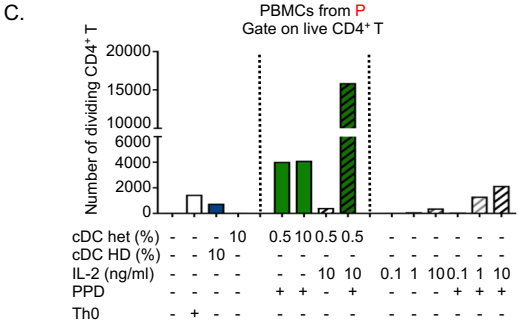

Supplemental Figure 9.

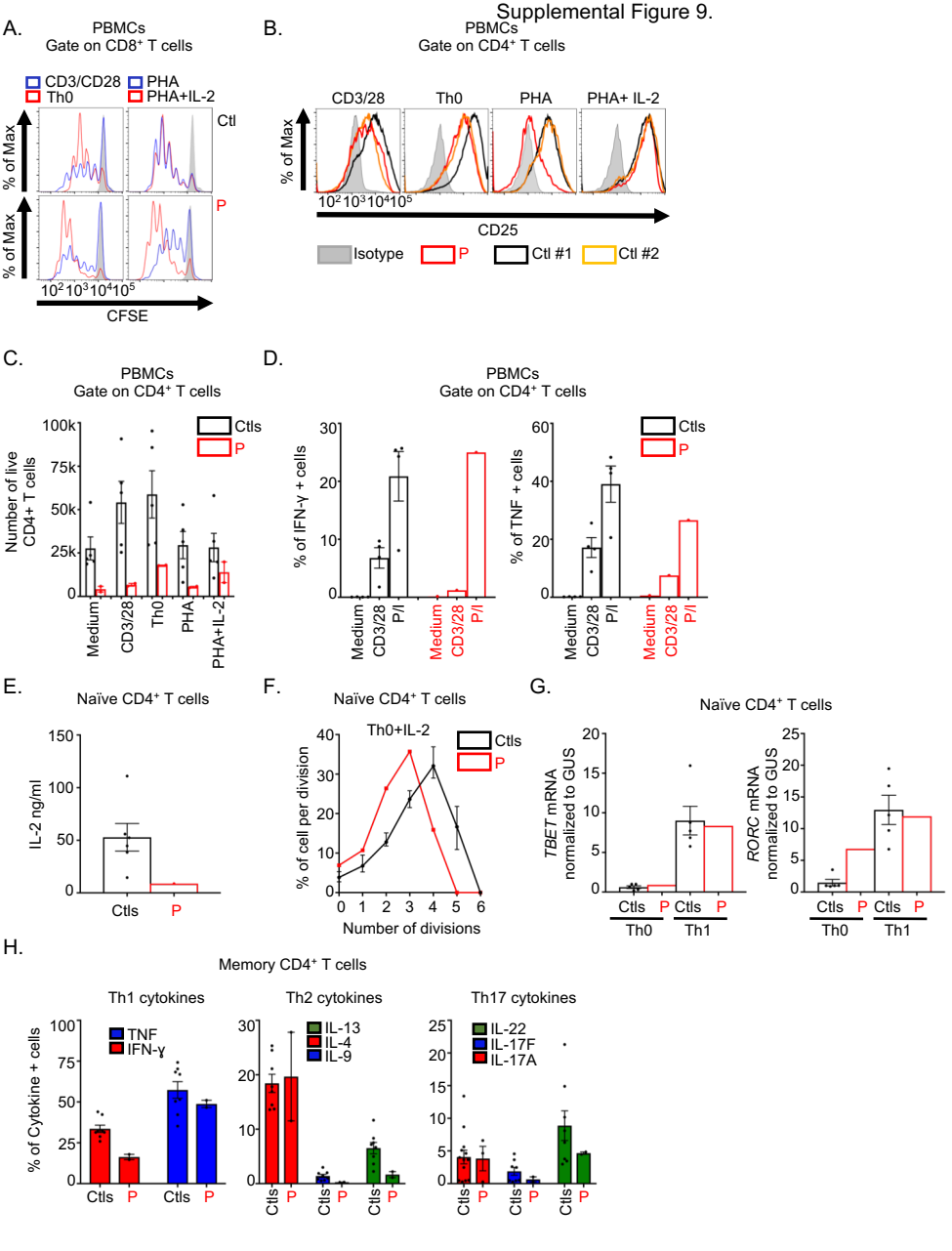

Supplemental Figure 10.

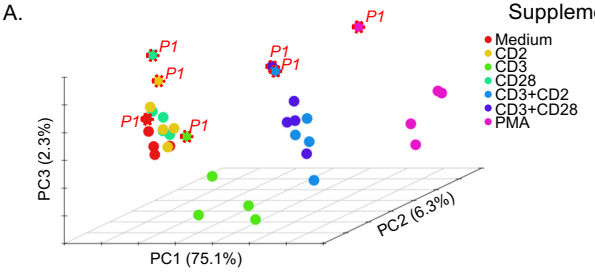

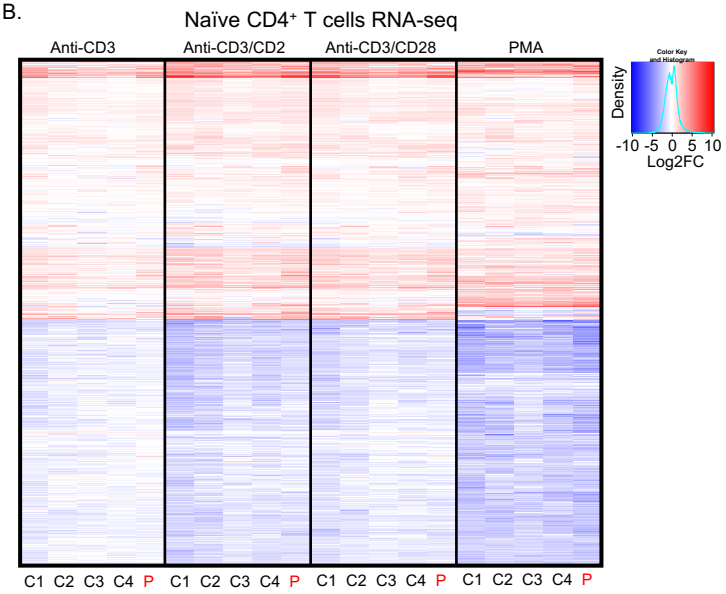

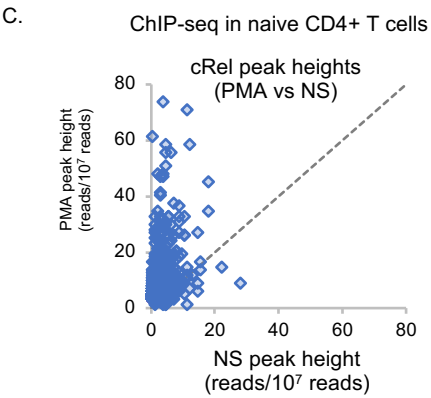

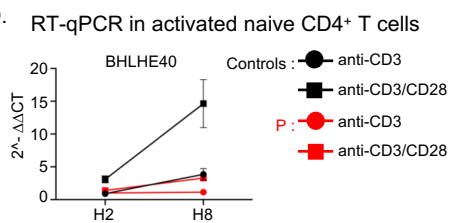

Supplemental Figure 11.

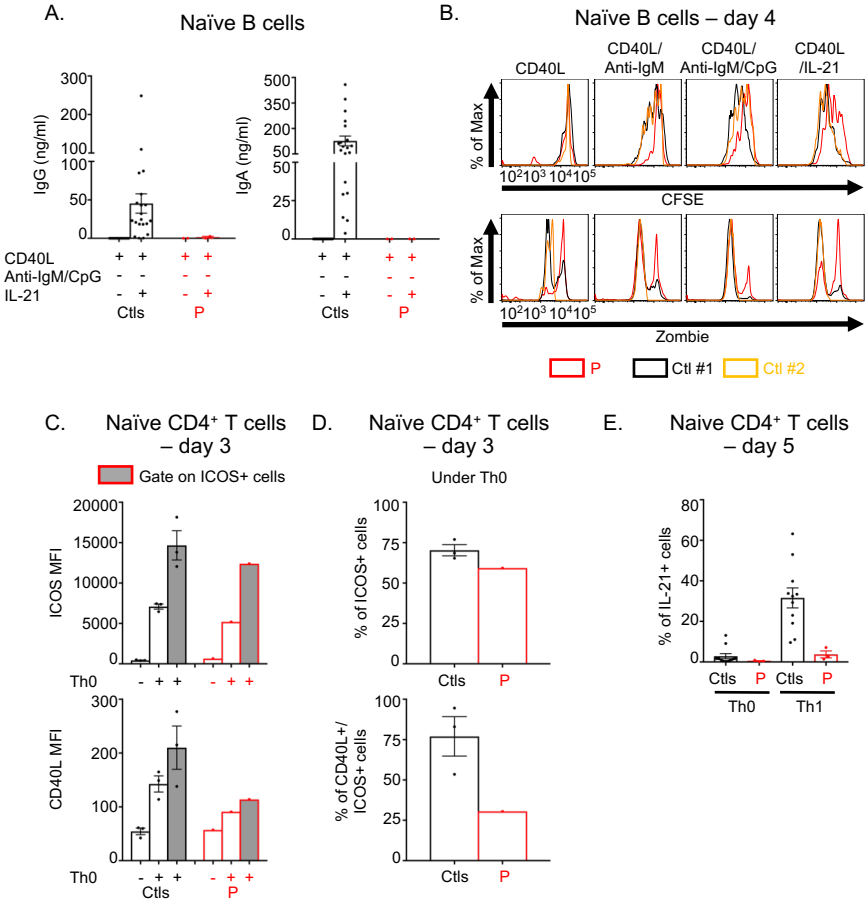

Supplemental Figure 12.

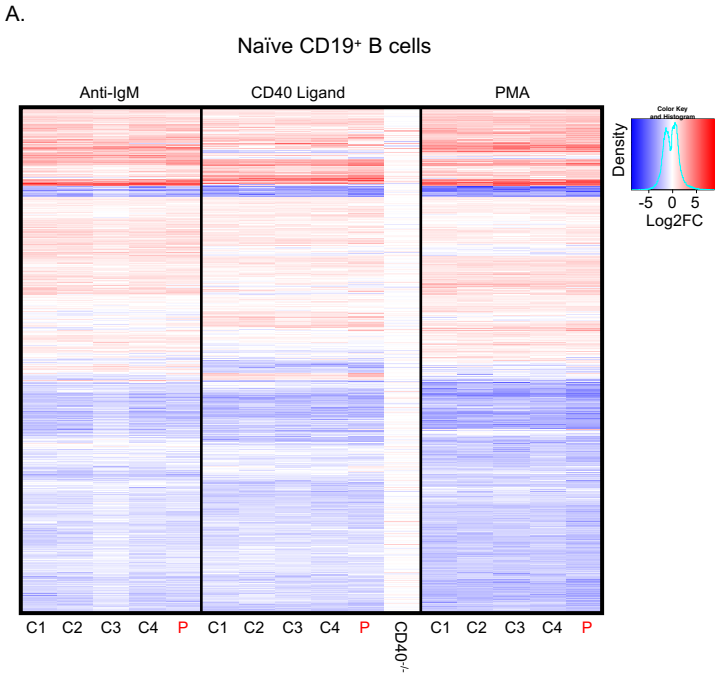

Methods

Sanger sequencing

The *REL* mutation was amplified from genomic DNA by PCR with the following primers: forward : ATCCCAGGTGAGGGGATAGT, reverse: AGTGATTATCTCTGGAGGATGAGA. The PCR products were sequenced with the BigDye Terminator Cycle Sequencing Kit (Applied Biosystems). Sequences were analyzed with an ABI Prism 3500 apparatus (Applied Biosystems).

Plasmids, directed mutagenesis and transient transfection

The pcDNA3.1 plasmid encoding N-terminally DDK-tagged human c-Rel was purchased from Addgene (#27253). The construct carrying the mutant allele was generated by direct mutagenesis with the QuikChange II XL Site-Directed Mutagenesis Kit (Agilent Technologies). HEK293T cells were transfected with a calcium phosphate kit (Thermo Fisher Scientific).

Cell lysis, and immunoblotting

Total protein extracts were prepared with lysis buffer (50 mM Tris pH7.4, 150 mM NaCl, 2 mM EDTA, 0.5% Triton X-100). Immunoblotting was performed with Abs against the N-terminus of c-Rel (D4Y6M, Cell Signaling Technologies), and monoclonal horseradish peroxidase-conjugated antibodies directed against FLAG (clone M2, Sigma-Aldrich), and GAPDH (FL335, Santa Cruz).

Luciferase reporter assay

NF-κB luciferase activity was assessed by transfecting HEK293T cells with 200 ng of NF-κB–dependent firefly luciferase plasmid with five NF-κB binding sites in the promoter (Agilent

Technologies), 40 ng of *Renilla* luciferase plasmid (pRL-SV40-d238), as an internal control, and a WT or mutant pcDNA3.1-REL-DDK plasmid (125 ng/well) in the presence of the X-tremeGENE 9 DNA Transfection Reagent (Roche). The cells were lysed in passive lysis buffer, and luciferase activities were measured in the Dual-Luciferase Reporter Assay (Promega).

Immunophenotyping of primary leukocytes by spectral flow cytometry

Thawed PBMCs (1.2×106 cells per panel) were stained with LIVE/DEAD Fixable Blue dye (Thermo Fisher Scientific) and blocked with FcR blocking reagent (Miltenyi Biotec) on ice for 15 minutes. After washing, cells were surface-stained with the following reagents on ice for 30 minutes: Brilliant Stain Buffer Plus (BD, Cat: 566385), anti-γδTCR-BUV661 (11F2, BD), anti-CXCR3-BV750 (1C6, BD), and anti-CCR4-BUV615 (1G1, BD). Cells were then washed and surface-stained with the following reagents on ice for 30 minutes: anti-CD141-BB515 (1A4), anti-CD57-FITC (HNK-1), anti-Vδ2-PerCP (B6), anti-Vα7.2-PerCP-Cy5.5 (3C10, BioLegend), anti-Vδ1-PerCP-Vio700 (REA173, Miltenyi Biotec), anti-CD14-Spark Blue 550 (63D3), anti-CD1c-Alexa Fluor 647 (L161), anti-CD66b-APC (G10F5), anti-CD38-APC-Fire 810 (HB-7), anti-CD27-APC H7 (M-T271), anti-CD127-APC-R700 (HIL-7R-M21), anti-CD19 Spark NIR 685 (HIB19), anti-CD45RA-BUV395 (5H9), anti-CD16-BUV496 (3G8,), anti-CD11b-BUV563 (ICRF44, BD), anti-CD56-BUV737 (NCAM16.2), anti-CD8-BUV805 (SK1, BD), MR1 tetramer-BV421, anti-CD11c-BV480 (B-ly6), anti-CD45-BV510 (HI30), anti-CD33-BV570 (WM53), anti-iNKT-BV605 (6B11), anti-CD161-BV650 (DX12, BD), anti-CCR6-BV711 (G034E3), anti-CCR7-BV785 (G043H7), anti-CD3-Pacific Blue (SK7,), anti-CD20-Pacific Orange (HI47), anti-CD123-Super Bright 436 (6H6), anti-Vβ11-PE (REA559, Miltenyi Biotec), anti-CD24-PE-Alexa Fluor 610 (SN3), anti-CD25-PE-Alexa Fluor 700 (3G10), anti-CRTH2-Biotin (BM16, Thermo Fisher Scientific), anti-CD209-PE-Cy7 (9E9A8), anti-CD117-PE-Dazzle 594 (104D2), anti-HLA-DR-PE-Fire 810

(L243), and anti-CD4-cFluor 568 (SK3). After washing, cells were further incubated with streptavidin-PE-Cy5 (BioLegend, 1:3000) on ice for 30 minutes. Cells were then washed, fixed with 1% paraformaldehyde (PFA)/PBS, washed again, and acquired with an Aurora cytometer (Cytek). Subsets were manually gated with FlowJo and further analyzed in R. The cellular composition was visualized through UMAP in R based on the expression levels of all available markers. Data were down-sampled to 50,000 cells per sample for visualization.

Flow cytometry of NK cell subsets

Immunophenotyping of NK cell subsets by flow cytometry was performed with Aqua Live/Dead Cell Stain Kit and mAbs against NKG2A (REA110, Miltenyi Biotech), KIR3DL1 (REA284, Miltenyi Biotec), CD7 (8H8.1, Beckman), CD57 (NK1,BD), NKG2C (REA205, Miltenyi Biotec), KIR2DL2-L3-S2 (GL183, Beckman), KIR2DL1-S1 (EB6, Beckman), CD3 (UCHT1, BD), CD16 (3G8, BD). Samples were analyzed with a Fortessa X20 (BD).

Phenotyping and functional analysis of innate lymphoid cells

PBMCs were stimulated with PMA (10 ng/ml; Sigma-Aldrich) plus ionomycin (1 µg/ml; Sigma-Aldrich) in the presence of Golgi-Plug (BD) for 3 h. Cells were surface-stained with mAbs against CD3 (UCHT1, eBioscience), CD4 (OKT4, eBioscience), CD5 (UCHT2, eBioscience), CD14 (TUK4, Miltenyi Biotec), CD19 (LT19, Miltenyi Biotec), TCR-αβ (IP26, eBioscience), TCR-γδ (B1.1, eBioscience), CD7 (M-T701, BD), CD56 (B159, BD), CD127 (eBioRDR5, eBioscience), CD117 (104D2, Biolegend). Cells were fixed, permeabilized with the Foxp3/TF Staining Buffer Set (eBioscience) and stained with intracellular mAbs against EOMES (WD1928, eBioscience), IFNγ (45-15, Miltenyi Biotec), GATA3 (TWAJ, eBioscience), IL-13 (JES10-5A2, BD). Samples were analyzed on an LSRFortessa machine (BD) and analyzed with FlowJo software (Tree

Star). ILCs were gated as Lin^- $CD7^+$ $CD56^-$ $CD127^+$ cells. Lineage staining (Lin) included staining for CD3, CD4, CD5, CD14, CD19, TCR-αβ and TCR-γδ. Within the ILC gate, ILC1 ($EOMES^-$ $IFN\gamma^+$), ILC2 ($GATA3^+$ $IL13^+$) and ILCP ($CD117^+$) were distinguished. All gated ILCs were $EOMES^-$.

Retrovirus production and transduction

The pLZRS-IRES-ΔNGFR (empty plasmid) and pLZRS-IRES-REL-ΔNGFR retroviral plasmids, both of which contain a puromycin resistance cassette, were generated as previously described(74). The ΔNGFR ORF encodes a truncated nerve growth factor receptor (NGFR, also known as CD271) protein incapable of signal transduction and serving as a cell surface tag. Briefly, Phoenix-A packaging cells were transfected with 10 μg of pLZRS-IRES-ΔNGFR or pLZRS-IRES-REL-ΔNGFR in the presence of X-tremeGENE 9 DNA reagent (Roche). Transfected cells were subjected to successive rounds of selection on puromycin (Gibco), at a concentration of 2 μg/ml, until all the cells expressed ΔNGFR on their surface, as shown by cell sorting with PE-anti-NGFR staining (BD). The Phoenix-A cell suspension was then split into two flasks, and the medium was replaced. After 24 h, the supernatant was collected and the retroviral particles were concentrated with a Retro-X concentrator (Clontech). We mixed 10 million EBV-B cells with the retrovirus-containing supernatant, in a total volume of 6 ml. Five days later, the stably transduced cells were purified by MACS, with a magnetic bead-conjugated anti-NGFR antibody (Miltenyi Biotec).

EBV-B and whole-blood activation

For the activation of EBV-B cells, 1 million EBV-B cells were seeded in a 24-well plate in a final volume of 1 ml RPMI supplemented with 10% FCS with PBDu (Sigma-Aldrich; 10^{-7} M) or PMA (400 ng/ml) per well, and the plate was incubated for 24 h at 37°C. For whole-blood activation

with BCG, 500 µl of fresh blood was added to each well of a 24-well plate and incubated for 48 h with BCG, IFN-γ (Imukin Boehringer Ingelheim; 10^5 IU/ml), or IL-12 (R&D Systems; 100 ng/mL). Supernatants were collected for ELISA according to the manufacturer's instructions for IL-12/IL-23p40 (R&D Systems), IL-12p70 (R&D Systems) IFN-γ (Sanquin) and TNF (Sanquin).

PBMC proliferation

Fresh PBMCs were labeled with CFSE (Invitrogen) and plated in 96-well plates (2.5 x 10^5/ml) in 200 µl RPMI supplemented with 10% FCS for four days with T-cell activation and expansion beads (Miltenyi Biotec), PHA (Sigma-Aldrich, #L2646, 1 µg/ml), 10 ng/ml rIL-2 (Thermo Fisher Scientific). Cells were collected and labeled with mAbs against CD8 (RPAT8, BD), CD3 (UCHT1, BD), and CD4 (RPA-T4, BD) and stained with LIVE/DEAD® Fixable Aqua stain. Proliferation was assessed by CFSE dilution.

Proliferation in allogeneic cocultures

Frozen $CD3^+$ T cells from healthy controls and P, and fresh conventional dendritic cells (cDCs) from various healthy controls were sorted with a FACS Aria II cytometer, using mAbs against CD16 (3G8, BD), CD14 (M5E2, Biolegend), HLA-DR (G46-6, BD), CD11c (B-ly6, BD), Nkp56 (9E2, Biolegend), CD56 (MY31, BD), CD19 (4G7, BD), CD15 (VIMC6, Miltenyi Biotec), CD3 (UCHT1, BD), and LIVE/DEAD® Fixable Aqua stain. Sorted $CD3^+$ T cells were stained with CFSE and added to 96-well plates (10^6/ml) in 200 µl of RPMI supplemented with 10% FCS per well. They were incubated with T-cell activation and expansion beads (Miltenyi Biotec) or with sorted cDCs (Lin^- $HLADR^+$ $CD14^-CD16^-CD11c^+$) at a 1:10 ratio for four days. Cells were collected and labeled with mAbs against CD8 (RPAT8, BD), CD3 (UCHT1, BD), CD4 (RPA-T4, BD) and stained with LIVE/DEAD® Fixable Aqua stain. Proliferation was assessed by CFSE dilution. For the

proliferation assay testing the response to tuberculin, frozen PBMCs from P were stained with CFSE and cultured with tuberculin in the presence of freshly sorted cDCs from P's mother, in various ratios. Proliferation was assessed after seven days.

Ex vivo naïve and effector/memory $CD4^+$ T-cell stimulation

$CD4^+$ T cells were labeled with anti-CD4, anti-CD45RA, anti-CCR7, anti-CD127 and anti-CD25 antibodies. Tregs ($CD4^+CD25^{hi}CD127^{lo}$) were excluded and naïve ($CD45RA^+CCR7^+$) T cells or effector/memory (defined as $CD45RA^-CCR7^+$) $CD4^+$ T cells were isolated (> 98% purity) with a FACS Aria machine (BD). Purified naïve or effector/memory $CD4^+$ cells were cultured with T-cell activation and expansion beads (Miltenyi Biotec) for 5 days. Culture supernatants were then used to assess secretion of the indicated cytokines, in cytometric bead array assays (BD) or by ELISA (Peprotech).

In vitro differentiation of naïve $CD4^+$ T cells

Naïve $CD4^+$ T cells ($CD45RA^+$ $CCR7^+$) were isolated from healthy controls, or P. Cells were cultured under polarizing conditions. Briefly, cells were cultured with T-cell activation and expansion beads (Miltenyi Biotec), alone or under Th1 (IL-12 [20 ng/ml; R&D Systems]), or Th17 (TGF-β [2.5 ng/ml; Peprotech], IL-1β [20 ng/ml; Peprotech], IL-6 [50 ng/ml; PeproTech], IL-21 [50 ng/ml; PeproTech], IL-23 [20 ng/ml; eBioscience], anti–IL-4 [5 μg/ml; DNAX], and anti-IFN-γ antibody [5 μg/ml; eBioscience]) polarizing conditions. After incubation for five days, the cells and culture supernatants were harvested and used to assess the secretion of the cytokines indicated, in cytometric bead array assays or by ELISA.

In vitro activation of B cells

Sorted naïve B cells were cultured in the presence of CD40L (200 ng/ml; R&D Systems), IL-21 (50 ng/ml; Peprotech), CpG 2006 (1 µg/ml; Sigma-Aldrich), and 0.01% SAC. The production of IgM, IgG and IgA was assessed by Ig heavy chain-specific ELISA on the culture supernatant after seven days. For proliferation and survival assays, sorted naïve B cells were stained with CFSE (Invitrogen). Proliferation was assessed by CFSE dilution, and viability was assessed by Zombie dye fixation (Biolegend), after five days.

In vitro derivation of dendritic cells and monocytes

Enriched bone marrow $CD34^+$ progenitor cell samples from healthy controls were purchased from StemCell Technologies and used for the derivation of dendritic cells and monocytes(75). Enriched bone marrow $CD34^+$ progenitor cell samples from P were prepared with the CD34 microbead kit (Miltenyi Biotec). The resulting preparation, enriched in $CD34^+$ cells, was then incubated with fluorescent mAbs against CD3 (OKT3, Biolegend), CD19 (HIB19, Biolegend), CD56 (HCD56, Biolegend), CD14 (TuK4, Invitrogen), CD66b (G10F5, Biolegend), CD303 (201A, Biolegend), CD11c (3.9, Biolegend), CD34 (581, Biolegend), CD45RA (HI100, Biolegend), and CD71 (CY1G4, Biolegend). Antibody-stained samples were then further purified by fluorescence-activated cell sorting (FACS) on the BD Influx. Sorted populations had a purity >95%. Specifically, hematopoietic progenitors (excluding $CD71^+$ erythroid precursors) were isolated as Lineage $(CD3/CD19/CD56/CD14/CD66b/CD303/CD11c)^-$ and $CD34^+$ $CD71^-$ cells. For stromal culture, MS5 stromal cells and OP9 stromal cells were maintained and passaged in complete α-MEM medium (Invitrogen) with 10% FCS and penicillin/streptomycin (Invitrogen). After three hours of treatment with 10 µg/ml mitomycin C (Sigma-Aldrich) and washing with PBS, 1.5×10^5 MS5 cells plus 2.5×10^4 OP9 cells per well were added to 24-well plates 24h before the culture of progenitor cells. Bulk $CD34^+$ $CD71^-$ progenitors (3000 cells per well) were

used to seed medium containing 100 ng/ml Flt3L (Celldex Therapeutics), 20 ng/ml SCF (PeproTech), and 10 ng/ml GM-CSF (PeproTech). Cells were cultured for two weeks, with replacement of half the medium every seven days of culture. Sorted populations of dendritic cells and monocytes were incubated for 48h with BCG, IFN-γ (Imukin Boehringer Ingelheim; 10^5 IU/ml), or LPS (10 µg/ml). Supernatants were collected for multiplex ELISA with a kit purchased from Mesoscale.

mRNA analysis and RT-qPCR

Total RNA was extracted with the RNeasy kit (Qiagen), and reverse-transcribed to generate cDNA. The cDNA for the *REL* full-length transcript was amplified with the following primers: forward: GGGTGCAAGAATTCAGGGGT, reverse: TCGCTATGTCCAAAGTTGTATGC. RT-qPCR was performed with the Applied Biosystems probe/primer specific for REL (Hs00968440_m1), BHLHE40 (Hs01041212_m1), IL2 (Hs00174114_m1), FOS (Hs04194186_s1), JUN (Hs01103582_s1), FOSL2 (Hs01050117_m1), FOSB (Hs00171851_m1), FOSL1 (Hs00759776_s1) and 13glucuronidase-VIC (4326320E), for normalization. Results are expressed according to the ΔCt method.

Exon trapping

In vitro exon trapping experiments were performed as previously described(76, 77). Briefly, a DNA segment encompassing a 3'-fragment of *REL* intron 4 (241 bp), exon 5 (141 bp), and a 5'-fragment of intron 5 (180 bp) was amplified from the genomic DNA of the patient and a control, and was inserted into pSPL3 (Life Technologies), between the *Xho*1 and *Not*1 sites. Wild-type (WT) and c.395-1G>A mutant clones (Mut) were used to transfect COS7 cells in the presence of X-tremeGENE 9 DNA Transfection Reagent (Roche). Total RNA was extracted with

the RNeasy Mini Kit (QIAGEN) and used for cDNA synthesis with the SuperScript III First-Strand Synthesis System (Life Technologies). SD6 and SA2 primers were used to amplify spliced transcripts from cDNA specimens by PCR. The PCR product was inserted into the pGEM-T Easy plasmid (Promega). About 100 clones were sequenced for each WT and Mut construct. SnapGene was used for sequence analysis.

REL TA cloning

The full-length cDNA generated from the EBV-B cells of a control and P was used for PCR amplification of exons 2 to 7 of *REL*, with the following primers: forward: TCCGGTGCGTATAACCCGTA, and the reverse: ACAATGGCTACTTGACGGTGT. The products obtained were cloned with the TOPO TA cloning kit (pCR2.1®-TOPO® TA plasmid, Thermo Fisher Scientific), and used to transform chemically competent bacteria. We subjected 100 clones per individual to Sanger sequencing with M13 primers (forward and reverse).

Stimulation of PBMCs with live BCG infection for cytokine production

PBMCs were plated at a density of 300,000 cells per well in 96-well U-bottomed plates, at a density of 1.5 x 10^6 cells/ml. Cells were plated in the presence and absence of live *M. bovis*-BCG at a MOI=1 (gift from Carl Nathan), and in the presence of recombinant IL-12 (5 ng/mL, R&D)(78). An additional well was included, to which no exogenous cytokine was added. After 39 h of culture, 50 ng/mL PMA and 1 µM ionomycin were added to this last well. One hour later, Golgiplug (BD) was added to each well, after 40 h of culture/stimulation. Cells were collected by centrifugation for flow cytometry staining. In brief, cells were first stained with the Zombie NIR Viability kit (BioLegend) for 15 minutes. They were then stained with FcBlock (Miltenyi Biotec), anti-γδTCR-alexa 647 (BioLegend), anti-CD3-V450 (BD), anti-CD56-BV605

(BioLegend), anti-CD4-BUV563 (BD), anti-Vδ1TCR-FITC (Miltenyi Biotec), anti-CD8-BUV737 (BD), anti-Vδ2TCR-APC/Fire750 (BioLegend), anti-CD20-BV785 (BioLegend), anti-Vα7.2-Alexa 700 (BioLegend), MR1-5-OP-RU-tetramer (NIH tetramer core facility), anti-Vβ11-APC (Miltenyi Biotec), and anti-iNKT-BV480 (BD) antibodies for 30 minutes. The stained cells were fixed with the FOXP3/Transcription Factor Buffer set (Thermo Fisher Scientific) and intracellularly stained with anti-T-bet-PE/Cy7 (BioLegend), anti-IFN-γ-BV711 (BioLegend), anti-TNF-α-BV510 (BioLegend), anti-IL-17A-PERCP/Cy5.5 and anti-RORγT-PE (BD) antibodies in Perm/Wash buffer. Cells were acquired on a CyTek Aurora spectral flow cytometer. Data were manually gated with FlowJo to determine the frequencies of IFN-γ^+ cell subsets. The cellular composition was visualized by Uniform Manifold Approximation and Projection (UMAP) in R, based on the expression levels of CD3, CD4, CD8, CD20, CD56, γδTCR, Vδ1 TCR, Vδ2 TCR, MR1 tetramer, Vα7.2 TCR, and T-bet. Technical duplicates, if any, were combined, and data were down-sampled to 10,000 cells per condition per individual.

Chromatin immunoprecipitation (ChIP)

Naïve B cells and naïve $CD4^+$ T cells were freshly isolated from three healthy donors PBMCs using Miltenyi Biotec columns (130-091-150; 130-094-131) and EBV-B cells were cultured in RPMI supplemented with 10% human serum. Cells were plated in 12-well plates in RPMI with 10% human serum and stimulated as follows for 2 h: B cells (NS, CD40L [100 ng/ml] and $F(ab')_2$ goat anti-human IgM [Jackson ImmunoResearch; 20 μg/ml], or PMA [40 ng/ml]; naïve $CD4^+$ T cells (NS or PMA); EBV-B cells (NS or PDBu [10^{-7} M]). ChIP was performed as previously described(79), with minor modifications. Briefly, cells were fixed by incubation with 1% formaldehyde in the culture medium for 10 minutes at room temperature. Crosslinking was stopped by adding 0.125 M glycine, cells were washed with cold PBS and nuclei were

extracted. Nuclei were resuspended in sonication buffer and the chromatin was sheared during four 30 s sonication cycles separated by intervals of 30 s, with a Bioruptor Pico (Diagenode); the sonicated fragments were 100-500 bp in size. Bead immunocomplexes were prepared by overnight incubation of 20 µl of Dynabeads Protein G and 20 µl of Dynabeads Protein A (Life Technologies) with 5 µg of anti-c-Rel antibody (D5G1A) or with a rabbit normal IgG control (2729S), both from Cell Signaling Technologies. Immunoprecipitation was performed by overnight incubation of the antibody-bead matrices with sheared chromatin from the equivalent of $2.5x10^6$ cells, followed by successive medium-stringency washes(80). Samples were de-crosslinked by overnight incubation at 65°C in 1% SDS buffer, followed by RNase A and proteinase K enzymatic treatments and were then subjected to DNA purification with the QIAquick PCR Purification kit (Qiagen). ChIP relative enrichment was assessed by qPCR analysis with PowerUp SYBR Green master mix (Thermo Fisher Scientific) with the primer sequences provided in Supplemental Table 10 ; enrichment within the NFKB1 and NFKBIA promoters was evaluated by the ΔΔCt method, using control IgG ChIP DNA as a negative control and the pro-opiomelanocortin (POMC) gene as a negative binding region. ChIP-seq libraries were prepared with the KAPA Hyperprep ChIP Library Preparation kit (Roche) and sequenced on one lane of an SP flow cell on an Illumina NovaSeq 6000 sequencer in a 50 bp paired-end read configuration. Input DNA for each cell type was sequenced as a negative control. The resulting sequence reads were assessed for quality with FastQC v0.11.8 (Babraham Bioinformatics); sequencing adapters and low-quality nucleotides were trimmed with Trimmomatic v.0.36(81) and then mapped to the hg38 human reference genome with Bowtie v1.1.2(82). c-Rel peak detection was performed with MACS v1.4.2(83), using a *p*-value threshold $<10^{-5}$; peak heights were retrieved with the Homer v4.11 annotatePeaks tool(84) and further filtered for a fold-enrichment >3 [ChIP vs Input], with peak heights >3 reads per

million retained. Sequence read density profiles (bigwig) with counts normalized per 10^7 reads were generated with the Homer tool and visualized with IGV(85). *De novo* motif enrichment analysis was performed with the Homer findMotifsGenome tool and visualized with WebLogo(86).

RNA sequencing

Total RNA was extracted from primary naïve $CD4^+$ T cells, naïve B cells and EBV-B cells with the RNeasy Plus Micro Kit (QIAGEN). RNA integrity and purity were evaluated using a Bioanalyzer 2100 (Agilent Technologies Genomics). cDNA was generated using the SMARTer v4 Ultra® Low Input RNA for Sequencing Kit (Takara Bio). Resulting cDNA was quantified and size controlled using a Bioanalyzer 2100 (Agilent Technologies Genomics). cDNA was normalized to 1 ng/ul and libraries were prepared using the Nextera XT DNA Library Preparation Kit (Illumina) and the Nextera XT Index Kit v2 set A (Illumina), respectively. 150 bp paired-end sequencing to approximately 20 million reads per sample was performed using a HiSeq4000 system (Illumina). Raw RNA-seq reads were aligned with UCSC human genome assembly version hg38, with STAR aligner(87). We used R version 3.5.2. We normalized the datasets with the functions DGEList and calcNormFactors from the DESeq2 version 1.22.2 package(88). We retained only genes with a count-per-million (CPM) greater than 10 in at least two samples. We considered a gene to be differentially expressed between two conditions if the log2-fold-change was greater than 1 (absolute value) and the adjusted *P*-value was below 0.05, according to the calculations made with the DESeq function. The raw and processed RNA-Seq data are available at the Gene Expression Omnibus (GEO), SuperSeries accession number GSE166873.

Single-cell RNA sequencing (scRNA-seq)

Single-cell RNA-seq profiling was performed on PBMCs obtained from P, the patient's mother, and healthy donors. PBMCs were quickly thawed at 37°C and resuspended by serial additions of DMEM + 10% heat-inactivated FBS. Cell counting and viability assessments were performed with the LIVE/DEAD™ Viability kit. The preparation was enriched in viable cells by resuspending one million cells in 200 µl of 1x PBS, 2% HI-FBS, 1mM $CaCl_2$, passing the suspension through a 40 µm Flowmi cell strainer (Sigma-Aldrich), and removing the dead cells with the EasySep Dead Cell Removal Kit (Stemcell Technologies). The final cell viability was 64% for the heterozygous sample and >90% for P and the healthy donors. The samples were loaded onto a 10X Genomics Chromium chip and reverse transcription and library preparation were performed with Chromium Single Cell 3' Reagent Kits (v3.1). Library quality was assessed with a Bioanalyzer DNA chip and the libraries were sequenced on one lane (S4 flowcell) of an Illumina NovaSeq 6000 sequencer. Sequence read quality was assessed with BVAtools (https://bitbucket.org/mugqic/bvatools). Cell Ranger v3.0.1 was used to map reads onto the hg38 human reference genome assembly, to perform filtering, and to count barcodes and unique molecular indices (UMIs). Genes that were not expressed in any of the datasets were discarded. Based on these counts, we extracted the summary statistics for the number of genes expressed per cell along with the summary statistics for the number of UMI per cell. Cells with >20% mitochondrial genes were excluded. We filtered out low-quality cells and doublets, by excluding cells falling outside the [-1 SD;+2.5 SD] interval for the UMI and gene count distribution. We further excluded doublets by manually removing cells co-expressing cell-specific markers (CD14, CD79A, TRBC1, HBA2 and LILRA4) and using the DoubletFinder package (89). We then analyzed P and healthy donors with the Seurat v3 R package (90) and cell clustering was performed by the Uniform Manifold Approximation and Projection

dimension reduction method (91) using the most variable genes, but excluding mitochondrial and ribosomal protein genes. The MAST approach (92) was used to identify the marker genes for each cluster and to perform the pairwise differential gene expression analysis comparing P and healthy donors.

Statistical analysis

Information on the statistical analyses is provided above for RNA-Seq and ChIP-Seq data.

Supplemental References

74. Martínez-Barricarte R, et al. Transduction of herpesvirus saimiri-transformed T cells with exogenous genes of interest. *Curr Protoc Immunol*. 2016;115:7.21C.1–7.21C.12.

75. Lee J, et al. Lineage specification of human dendritic cells is marked by IRF8 expression in hematopoietic stem cells and multipotent progenitors. *Nat Immunol.* 2017;18(8):877–888.

76. Nisson PE, et al. Isolation of exons from cloned DNA by exon trapping. *Curr Protoc Hum Genet*. 2001;Chapter 6:Unit 6.1.

77. Belkaya S, et al. Autosomal recessive cardiomyopathy presenting as acute myocarditis. *J Am Coll Cardiol*. 2017;69(13):1653–1665.

78. Vogt G, Nathan C. In vitro differentiation of human macrophages with enhanced antimycobacterial activity. *J Clin Invest*. 2011;121(10):3889–3901.

79. Langlais D, et al. The Stat3/GR interaction code: predictive value of direct/indirect DNA recruitment for transcription outcome. *Mol Cell*. 2012;47(1):38–49.

80. Langlais D, et al. The macrophage IRF8/IRF1 regulome is required for protection against infections and is associated with chronic inflammation. *J Exp Med*. 2016;213(4):585–603.

81. Bolger AM, et al. Trimmomatic: a flexible trimmer for Illumina sequence data. *Bioinformatics*. 2014;30(15):2114–2120.

82. Langmead B, et al. Ultrafast and memory-efficient alignment of short DNA sequences to the human genome. *Genome Biol*. 2009;10(3):R25.

83. Zhang Y, et al. Model-based analysis of ChIP-Seq (MACS). *Genome Biol*. 2008;9(9):R137.

84. Heinz S, et al. Simple combinations of lineage-determining transcription factors prime cis-regulatory elements required for macrophage and B cell identities. *Mol Cell*. 2010;38(4):576–589.

85. Thorvaldsdóttir H, et al. Integrative Genomics Viewer (IGV): high-performance genomics data visualization and exploration. *Brief Bioinform*. 2013;14(2):178–192.

86. Crooks GE, et al. WebLogo: a sequence logo generator. *Genome Res*. 2004;14(6):1188–1190.

87. Dobin A, et al. STAR: ultrafast universal RNA-seq aligner. *Bioinformatics*. 2013;29(1):15–21.

88. Love MI, et al. Moderated estimation of fold change and dispersion for RNA-seq data with DESeq2. *Genome Biol*. 2014;15(12):550.

89. McGinnis CS, et al. DoubletFinder: doublet detection in single-cell RNA sequencing data using artificial nearest neighbors. *Cell Syst*. 2019;8(4):329–337.

90. Stuart T, et al. Comprehensive integration of single-cell data. *Cell*. 2019;177(7):1888–1902.

91. Becht E, et al. Dimensionality reduction for visualizing single-cell data using UMAP. *Nat Biotechnol*. 2019;37(1):38–44.

92. Finak G, et al. MAST: a flexible statistical framework for assessing transcriptional changes and characterizing heterogeneity in single-cell RNA sequencing data. *Genome Biol*. 2015;16(1):278.

93. Banerjee D, et al. c-Rel-dependent priming of naive T cells by inflammatory cytokines. *Immunity*. 2005;23(4):445–458.

94. Visekruna A, et al. c-Rel is crucial for the induction of Foxp3(+) regulatory CD4(+) T cells but not T(H)17 cells. *Eur J Immunol*. 2010;40(3):671–676.

95. Ruan Q, et al. The Th17 immune response is controlled by the Rel-RORγ-RORγ T transcriptional axis. *J Exp Med*. 2011;208(11):2321–2333.

96. Long M, et al. Nuclear factor-kappaB modulates regulatory T cell development by directly regulating expression of Foxp3 transcription factor. *Immunity*. 2009;31(6):921–931.

97. Ruan Q, et al. Development of Foxp3(+) regulatory t cells is driven by the c-Rel enhanceosome. *Immunity*. 2009;31(6):932–940.

98. Liou HC, et al. c-Rel is crucial for lymphocyte proliferation but dispensable for T cell effector function. *Int Immunol*. 1999;11(3):361–371.

99. Tumang JR, et al. c-Rel is essential for B lymphocyte survival and cell cycle progression. *Eur J Immunol*. 1998;28(12):4299–4312.

100. Heise N, et al. Germinal center B cell maintenance and differentiation are controlled by distinct NF-κB transcription factor subunits. *J Exp Med*. 2014;211(10):2103–2118.

101. Stankovic S, et al. Distinct roles in NKT cell maturation and function for the different transcription factors in the classical NF-κB pathway. *Immunol Cell Biol*. 2011;89(2):294–303.

102. Boffa DJ, et al. Selective loss of c-Rel compromises dendritic cell activation of T lymphocytes. *Cell Immunol*. 2003;222(2):105–115.

103. O'Keeffe M, et al. Distinct roles for the NF-kappaB1 and c-Rel transcription factors in the differentiation and survival of plasmacytoid and conventional dendritic cells activated by TLR-9 signals. *Blood*. 2005;106(10):3457–3464.

Full unedited gel for Figure 2C

Anti-DDK

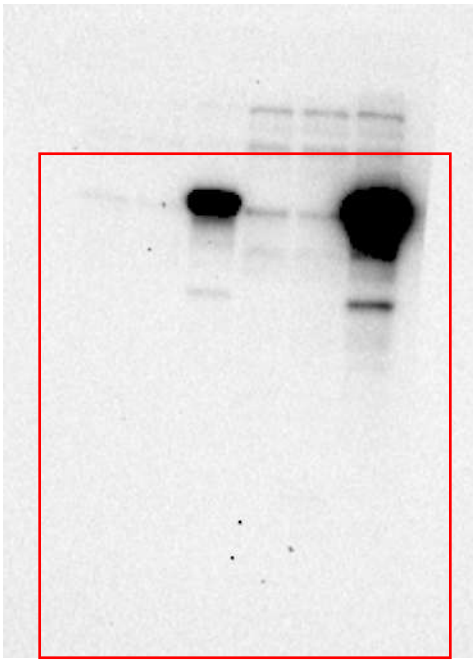

Anti-GAPDH

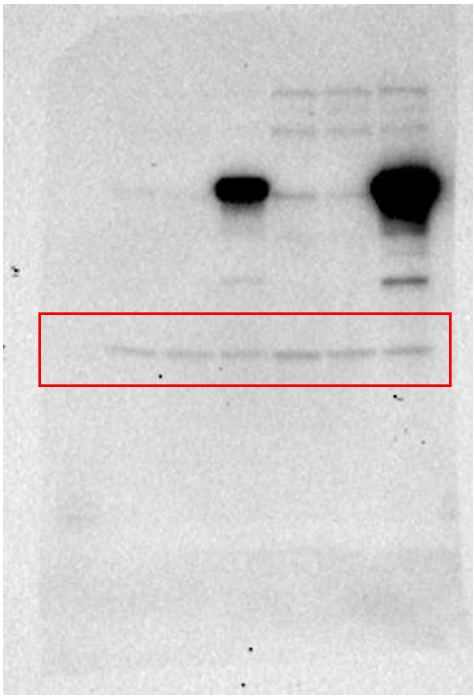

Full unedited gel for Supplemental Figure 3A

Anti-c-Rel

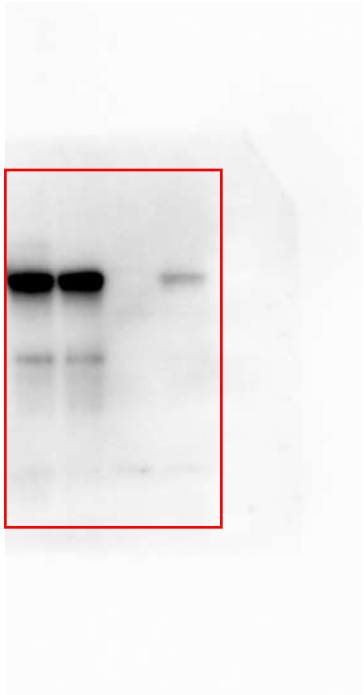

Anti-GAPDH